DETERMINATION OF THE EARTH'S STRUCTURE

Literature

Bullen, K.E. & Bolt, B.A. 1985. <u>An Introduction to the Theory of Seismology</u>. Cambridge University Press, 4th edition.

Kijko, A. 1996. <u>Statistical Methods in Mining Seismology</u>. South African Geophysical Association.

Lay, T. & Wallace, T.C. (1995). <u>Modern Global Seismology</u>. Academic Press, Inc., 517 pages.

INTRODUCTION

The answer to geodynamical questions is commonly linked to the knowledge of the Earth's interior. Depending on the scale of the object to be investigated, several inversion methods can employed.

lw0701
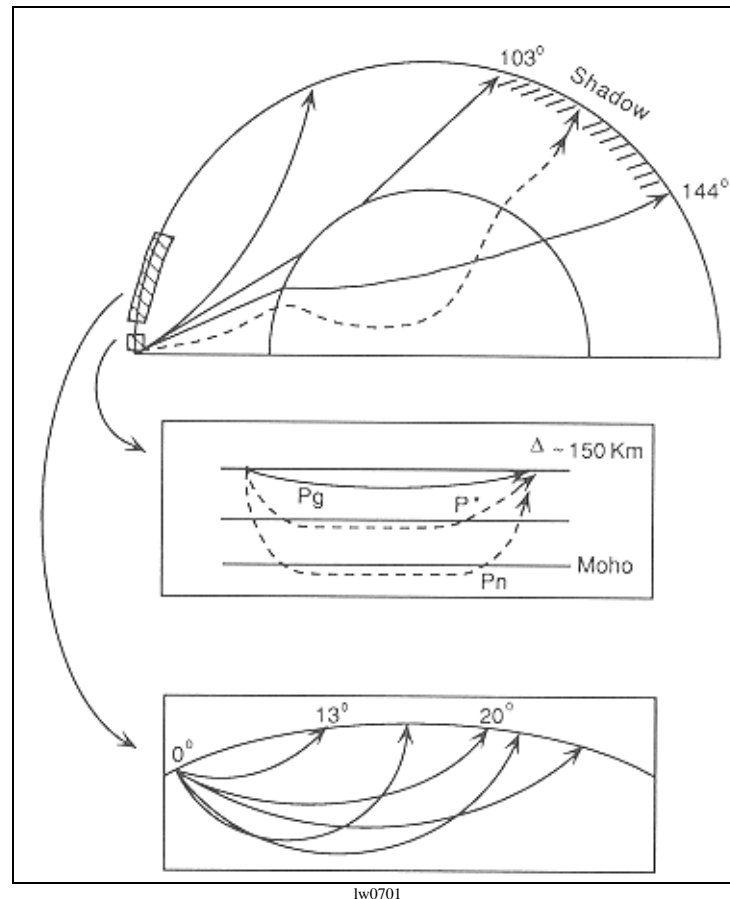
Schematic diagram of three characteristic distance ranges used in the study of the Earth's structure (from Lay, T. & Wallace, T.C. 1995. Modern global seismology. Academic Press, Inc.).

The distance ranges are:
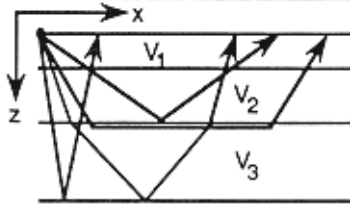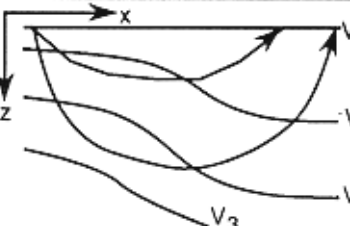
1. near to regional = 0 km - 1400 km (0° - 13°), crustal phase (figure in the middle)
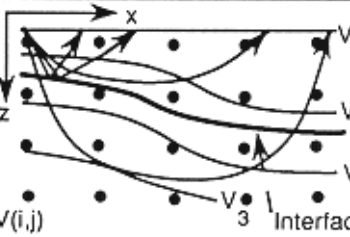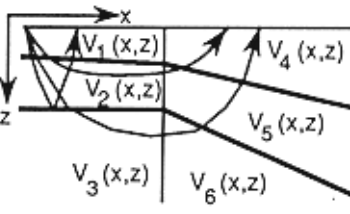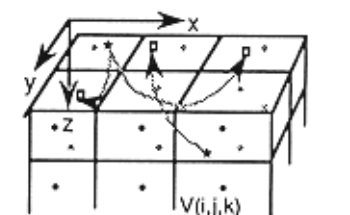
2. upper-mantle = 1400 km - 3300 km (13° - 30°), upper-mantle triplication signals (bottom figure)

3. teleseismic = > 3300 km (30° - 180°), penetrates core and lower mantle and reverberates in upper mantle (figure at the top)

INVERSION METHODS

Inversions techniques allow to reconstruct a physical model from observations. The antinomy is 'forward modelling'.

We distinguish three basic types of inversions:
1. Analytic Inversion (Herglotz-Wiechert) and Discrete Inversions
2. Iterative Inversions (Tomography)
3. Attenuation Modelling (intrinsic inelasticity and attenuation as a result of scattering)

Method/Para-meterization	Dim.	Model Illustration	Observed Data (Phases)
A. T-X Inversion; Homogeneous Layers	1-D		Refracted and Reflected Arrivals
B. Tau-p, Extremal Inversion; Slant Stack; V(z) inversion	1-D		Refractions, (Wide-angle Reflections)
C. Iterative Ray Trace, V(x,z) Polynomial	2-D		Refractions
D. Iterative Ray Trace, Velocity defined at node points (V(i,j)), Interfaces may be included	2-D		Refractions and Reflections
E. Iterative Ray Trace, Velocity model defined by blocks and interfaces, V(z) within blocks	2-D		Refractions and Reflections
F. Iterative Ray Trace, Velocity defined by homogeneous blocks or interpolated from nodes, V(i,j,k)	3-D		Controlled Source and Earthquake arrival times; Teleseismic delay times (transmitted case)

tomo1

HERGLOTZ-WIECHERT

This method is based on articles by Batemann, Herglotz and Wiechert[1] and utilizes the constant ray parameter 'p':

$$p = \frac{\sin i}{c}$$

$$\sin i = \frac{dx}{ds} = cp$$

$$\cos i = \frac{dz}{ds} = \sqrt{1 - \sin^2 i} = \sqrt{1 - c^2 p^2}$$

$$dx = ds \sin i = \frac{dz}{\cos i} cp = \frac{cp}{\sqrt{1 - c^2 p^2}} dz$$

Hence, the distance 'X', where the ray emerges at the surface, depends on 'p' and is given by

$$X(p) = 2 \int_0^z \frac{cp}{\sqrt{1 - c^2 p^2}} dz$$

The travel time 'T' of a seismic ray between a source at the surface and a receiver at the surface - separated by the distance 'X' - is given by

$$dT = \frac{ds}{c} \Rightarrow T = 2 \int_0^s \frac{ds}{c(s)} = 2 \int_0^z \frac{dz}{c(z) \cos i}$$

$$T(p) = 2 \int_0^z \frac{dz}{\sqrt{1 - c^2 p^2}}$$

with s = ray path, c = propagation velocity at depth 'z', x = distance at surface.

[1]Batemann, H. 1910. Die Lösung der Integralgleichung, welche die Fortpflanzungsgeschwindigkeit einer Erdbebenwelle im Inneren der Erde mit den Zeiten verbindet, die die Störung braucht, um zu verschiedenen Stationen auf der Erdoberfläche zu gelangen. Physikal. Zeitschr., Bd. 11, 96-99.

Herglotz, G. 1907. Über das Benndorf'sche Problem der Fortpflanzungsgeschwindigkeit der Erdbebenstrahlen. Physikal. Zeitschr., Bd. 8, 145-147.

Wiechert, E. & Geiger, L. 1901. Bestimmung des Weges von Erdbebenwellen im Erdinneren. Physikal. Zeitschr., Bd. 11, 394-411.

Wiechert, E. 1910. Bestimmung des Weges von Erdbebenwellen. I. Theoretisches. Phys. Z., 11, 294-304.

The latter integral can be split into two terms:

$$T(p) = 2\int_0^z \frac{dz}{\sqrt{1-c^2 p^2}} = 2\int_0^z \frac{\frac{1}{c^2}}{\sqrt{\frac{1}{c^2} - p^2}} dz =$$

$$2\int_0^z \left(\frac{p^2}{\sqrt{\frac{1}{c^2} - p^2}} + \sqrt{\frac{1}{c^2} - p^2} \right) dz =$$

$$T(p) = pX(p) + 2\int_0^z \left(\sqrt{\frac{1}{c^2} - p^2} \right) dz$$

The first term depends only on the surface distance 'X' and the other on the depth 'z'. Note, that the ray parameter 'p' is therefore alternatively referred to as 'horizontal slowness' (p = dT/dX).

Further, we note that the ray parameter 'p' equals the '$1/c_b$' at the maximum penetration depth 'z', for sin $i = 1$ for horizontal rays, with 'c_b' as the phase velocity at the bottom (turning point) of the ray.

Assuming the following restrictions,

1. all layers are parallel (= no horizontal velocity gradient)
2. all elastic constants are only dependent on depth (s.a. point 1.)
3. the change of the velocity gradient is always positive (= no low-velocity layers; they can be introduced later by the 'stripping method', s.a. Lay & Wallace[2])

we may determine maximum penetration depth of a particular ray from its ray parameter 'p' and its associated phase velocity 'c_b' (=1/p). The following procedure is referred to as the '*Herglotz-Wiechert Inversion*'.

We may rewrite

$$X(p) = 2\int_0^z \frac{cp}{\sqrt{1-c^2 p^2}} dz$$

as

$$\frac{X}{2} = \int_0^{z_b} \frac{c}{\sqrt{1 - \frac{c^2}{c_b^2}}} dz \Rightarrow \frac{X}{2} c_b = \int_0^{z_b} \frac{dz}{\sqrt{\frac{1}{c^2} - \frac{1}{c_b^2}}}$$

---

[2] Lay, T. & Wallace, T.C. 1995. Modern Global Seismology. Academic Press, Inc., page 240.

To determine the velocity distribution under the integral, we may use Abel's integral solution([3], after [4]):

$$f(\eta) = \int_{\eta}^{a} \frac{u(\xi)}{(\xi - \eta)^{\lambda}} d\xi$$

with the solution

$$u(\xi) = \frac{\sin \lambda \pi}{\pi} \frac{d}{d\xi} \int_{\xi}^{a} \frac{f(\eta)}{(\eta - \xi)^{1-\lambda}} d\eta$$

Substituting

$$\frac{1}{c^2} = \xi$$

$$\frac{1}{c_b{}^2} = \eta$$

we get

$$\frac{X}{2} c_b = \int_{\xi = \frac{1}{c_0{}^2}}^{\xi = \eta} \frac{dz}{d\xi} \frac{d\xi}{(\xi - \eta)^{1/2}}$$

for which Abel's solution is

$$\frac{dy}{d\xi} = \frac{1}{2\pi} \frac{d}{d\xi} \int_{\xi}^{1/c_0{}^2} \frac{xc_b}{(\eta - \xi)^{1/2}} d\eta$$

which leads to

$$\kappa = \frac{\left(\frac{\partial X}{\partial T}\right)_X}{\left(\frac{X}{T}\right)}, \; z(X) = \frac{1}{\pi} \int_0^X \ln\left(\kappa + \sqrt{\kappa^2 - 1}\right) dx, \; v(z(X)) = \left(\frac{\partial X}{\partial T}\right)_X$$

The integral is numerically evaluated with discrete values of the change of the slope of the travel time curve. Note, 'X/T' = apparent velocity, $\delta X/\delta T_X$ = change in slope of travel-time curve at distance 'X'.

---

[3] Abel, N.H.: Norwegian mathematician, 1802 - 1829.

[4] Meissner, O. 1929. Beiträge zu einer experimentellen Seismik. Veröff. D. Reichsanstalt f. Erdbebenforschung in Jena, Heft 9.

TOMOGRAPHY

tomo = 'slice' (greek)

Definition (aiming at travel time tomography[5]):
'Tomography can be defined as the reconstruction of a field from the knowledge of linear path integrals through the field. In seismology, the analysis of lateral velocity variations fits this definition, if the travel time equation is perturbed about a reference velocity model. The field in this case is slowness perturbations, and the observations are travel time deviations.'

1917	Johann Radon (Austrian mathematician)	Central Slice Theorem: Reconstruction of 2D-image from set of 1D-integrals, or reconstruction of 3D-image from 2D-slices
1963	Alan M. Cormack (South Africa/U.S.A.)	'Representation of a Function by its Line Integrals with some Radiological Applications' $$I = I_0 \exp\left[-\int_L g(l)dl\right], \ln\left(\frac{I_0}{I}\right) = \int_L g(l)dl, f_L = \ln\left(\frac{I_0}{I}\right)$$ $$f_L = \int_L g(l)dl$$
1971	Sir Geoffrey N. Hounsfield (British engineer)	First application (combination of X-ray scanner and computer)
1979	Cormack and Hounsfield	Nobel prize for 'Development of computer assisted tomography - (CAT scan)'

Comparison

	Radiology	**Seismology**[6]
Equation	$$f_L = \int_L g(l)dl$$	$$t_L = \int_L s(l)dl$$
Unknown	g(l) = absorption coefficient	s(l) = slowness = 1/velocity
Ray path	L is a straight line	L is usually not straight
Sources	known	usually unknown
Detectors	many and controllable	few and not optimally placed
Verification	easy	difficult
Funding	well funded	poorly funded

---

[5] Clayton, 1984. Seismic Tomography (abstract). Eos, Trans.Am.Geophys.Union, Vol.65, 236.
[6] Note: The formula applies to travel time-tomography.

TRAVEL TIME TOMOGRAPHY

> Use (general):
> Seismic tomography is used to map velocity- and density contrasts to find geological structures, caverns and stress anomalies. Repetition of tomographic imaging allows to identify regions of fast-changing stress conditions and to monitor the efficiency of stress release operations.

Travel time tomography[7] calculates the spatial slowness 's_j' from individual travel times 't_i' (each travel time is a result of a unique ray with index 'i') thus giving an impression of spatial velocity perturbations.

$$t_i = \int_{L_i} s_j \, dl$$

Problem: The ray path depends on the unknown slowness 's'. The equation stated above, is therefore non-linear in respect to 's'.

Solution: Linearizing about an initial slowness-model $s(x,y,z) = s_0(x,y,z) + \delta s(x,y,z)$, and solving for perturbations of δs (see 'ACH' and 'NeHT' later).

$$\delta t_i = \int_{L_i} \delta s_j \, dl \qquad \text{or} \qquad \delta t_i = \sum_{j=1}^{m} l_{ij} \delta s_j$$

where δt_i is the time delay of the i-th ray, δs_j is the slowness perturbation of the j-th block, and l_{ij} is the length of the i-th ray in j-th block. Note: 'm' is not a constant, for each ray may cross a different number of blocks.
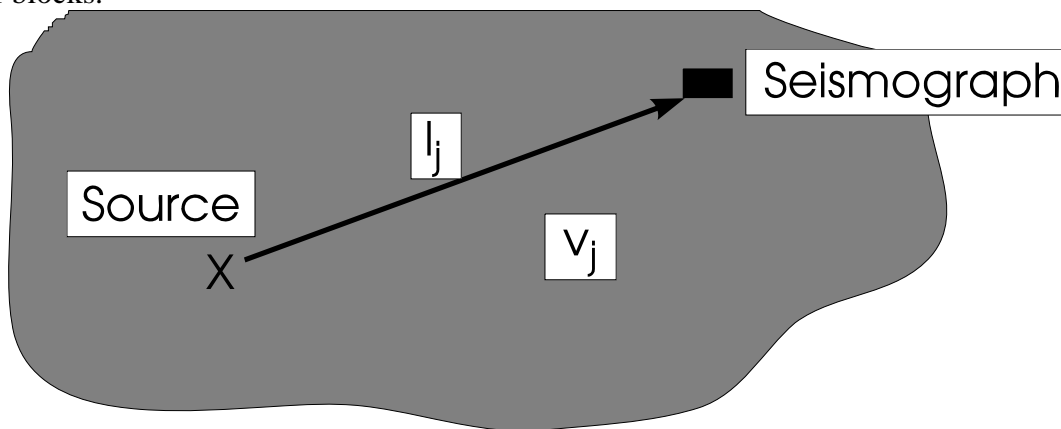
$$t = \int_{ray \; path} \frac{1}{v_{x,y}} dl \longrightarrow \sum_{j}^{N_{cells}} \frac{l_j}{v_j} = \sum_{j}^{N_{cells}} l_j s_j \; with \; s_j = \frac{1}{v_j}$$

Basic tomographic equation:

$$\mathbf{t} = \mathbf{L} \, \mathbf{s}$$

with t = vector of travel times of each ray, L = matrix of travel paths, s = slowness vector. Note: Bold letters denote matrices

---

[7]Kijko, A. 1996. Statistical methods in mining seismology. South African Geophysical Association.

Algebraic Reconstruction Technique (ART)

This iterative method was used originally in biological and medical sciences since 1939 (method proposed by Kaczmarc), reinvented and given the new name ART. In geophysics the method is used since 1983 (McMechan). The method is rather unstable. Therefore linearization techniques have been introduced.

ART-Procedure[8]:

1. Subdivide model into m-cells, represented by rows and columns (m = rows * columns)
2. Each cell is allocated a unique index (e.g. j = (row-index-1)*columns + column-index)
3. Guess initial approximation of δs_j *(j = 1..m) for each seismic ray i (i = 1..n)
4. Compute all i-th ray segments l_{ij} (if they differ from the previous iteration) and residuals
   r_i *= δt_i - $\Sigma l_{ij} \delta s_j$*
5. Adjust δs_j according to

$$\delta s_j = \delta s_j^* + \frac{l_{ij} r_i^*}{\sum_k l_{ik}^2}$$

   These values are now applied to the next ray.
6. Return to point (4) until a termination criteria is met.

This iteration process depends on the order at which the rays are considered! To improve the convergence Dines and Lytle (1979)[9] suggest computing the corrections for all rays first, keeping the residuals fixed, and averaging these corrections before updating δs. The equation at step 5 of the procedure is then replaced by

$$\delta s_j = \delta s_j^* + \frac{1}{n_j} \frac{\sum_j l_{ij} r_i^*}{\sum_k l_{ik}^2}$$

with n_j = number of rays passing through block j and all other values remain fixed!

Methods in which the solution is updated only after <u>all rays</u> (= equations) have been processed, are called **Simultaneous Iterative Reconstruction Techniques (SIRT).**

Least Square Reconstruction (LSQR) or Inversion without blocks

LSQR[10] is a conjugate gradient method which is powerful to solve large sparse systems (matrix **L** is usually ill-conditioned). The method is fast and accurate. It avoids calculating eigenvectors from the matrix $\mathbf{L}^T\mathbf{L}$, which is extremely bad conditioned, by employing normal equations $\mathbf{L}^T\mathbf{L}\delta\mathbf{s} = \mathbf{L}^t\delta\mathbf{t}$. Further, the method is based on the Bayesian premise thus making use of probability theory.

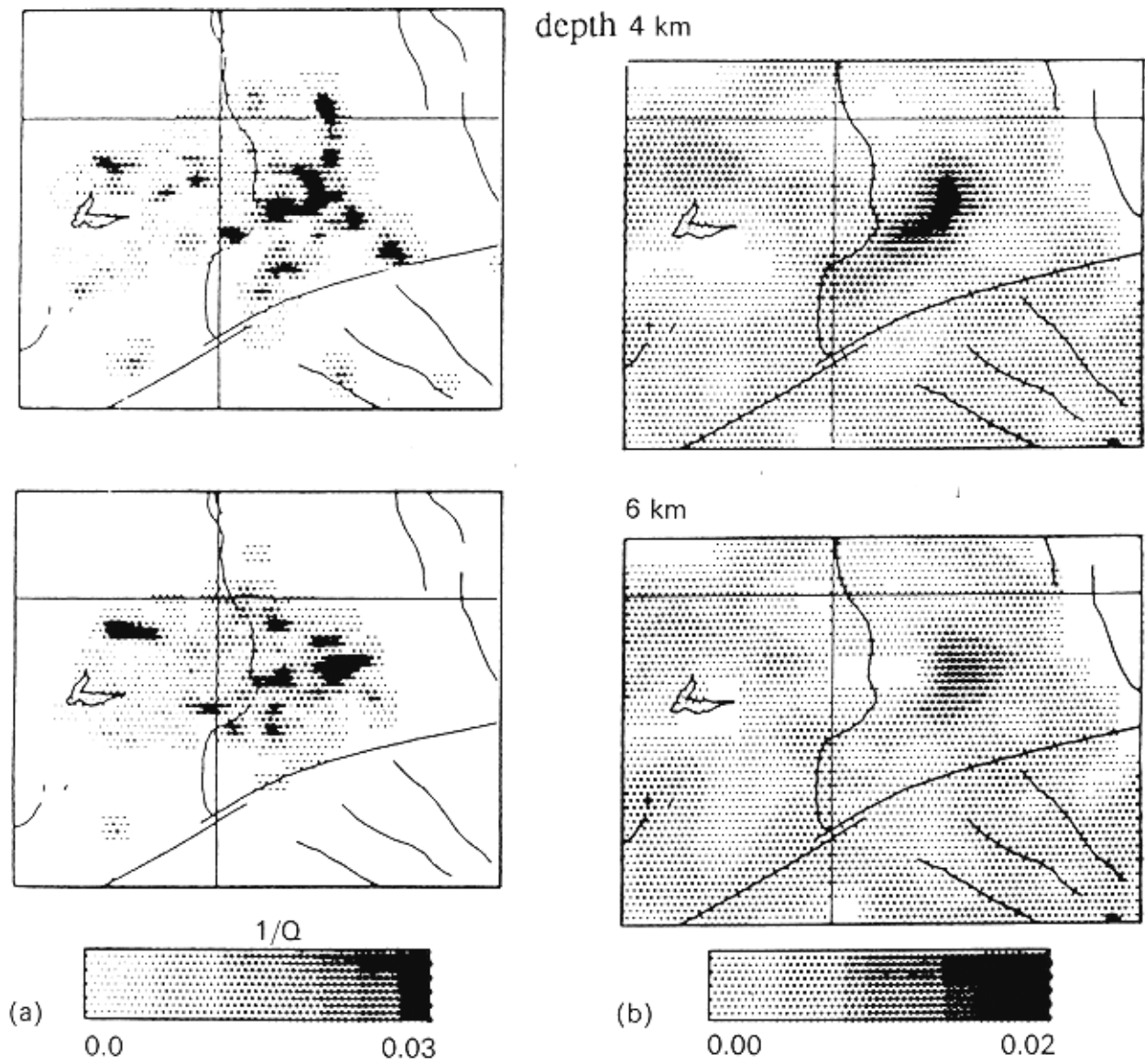
[8] Kijko, A. 1996. Statistical methods in mining seismology. South African Geophysical Association.

[9] Dines, K.A. & Lytle, J.R. 1979. Computerized Geophysical Tomography. Proc. of IEEE, Vol.67, No.7, 1065-1073.

[10] Nolet, G. 1993. Solving large linearized tomographic problems. In 'Seismic Tomography' (Iyer & Hirahara, eds.), Chapman & Hall, 227-247.

Comparing SIRT with LSQR

Q-model derived from data inverted with SIRT (left) and with LSQR (right) at two depth levels (Nolet, G. 1993[11]).

---

[11] Nolet, G. 1993. Solving large linearized tomographic problems. In 'Seismic Tomography' (Iyer & Hirahara, eds.), Chapman & Hall, 227-247.

ACH

The ACH inversion method (named after the authors[12]) is the oldest and perhaps the most robust seismic tomography technique. It applies to 'restricted-array' problems, that is, when all receivers are remote from the source. Hence, the method lends itself for studies of local crustal properties beneath an array of receivers, derived from relative time differences of teleseismic signals.

The ACH inversion is based on the linearization of the integral of relative travel time residuals:

$$\Delta r_{ij} = r_{ij} - \frac{1}{n_i} \sum_{j=1}^{n_i} r_{ij}$$

$$= \int_L \Delta s ds - \frac{1}{n_i} \sum_{j=1}^{n_i} \int_L \Delta s ds$$

with Δs = relative slowness residuals, n_i = number of stations recording the i-th earthquake, and L = ray path within the model.


lw0704
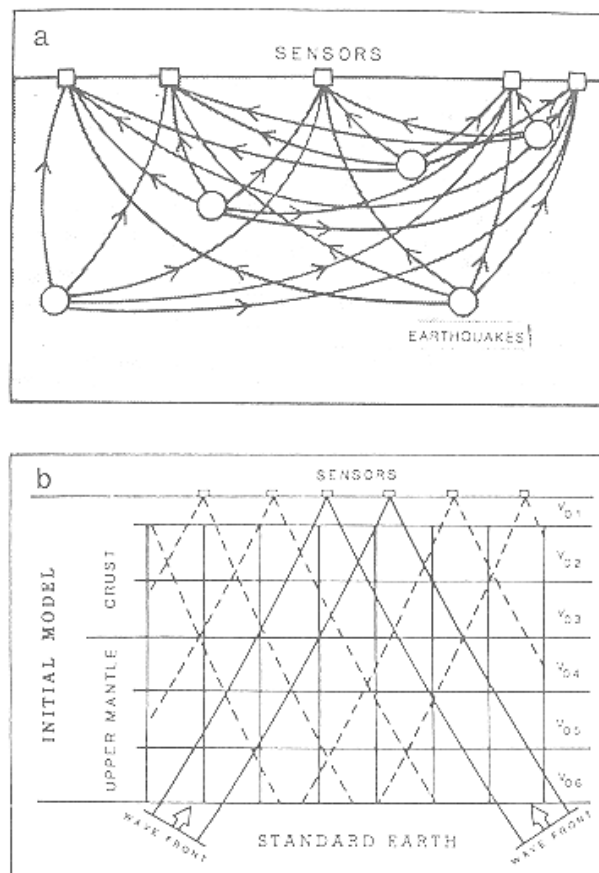
Restrictions are:

1. Signals from beyond 25° of distance should be discarded to avoid problems associated with the presumed standard Earth model.
2. Receiver stations should be evenly spread.

A special case of ACH is called NeHT (also named after the authors).

---

[12] Aki, K., Christoffersson, A. & Husebye, E.S. 1977. Determination of the three-dimensional structure of the lithosphere. J.Geophys.Res., 82, 277-296.
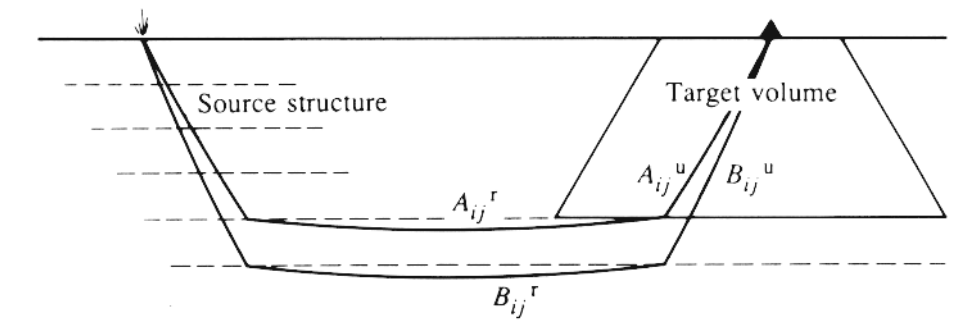
NeHT

The NeHT inversion method (named after the authors[13]) can be understood as a high-resolution tomography based on the ACH-approach - but utilizing active sources. The method is widely employed to investigate physical properties and geometries of the Earth's crust such as volcanoes[14] and salt domes.
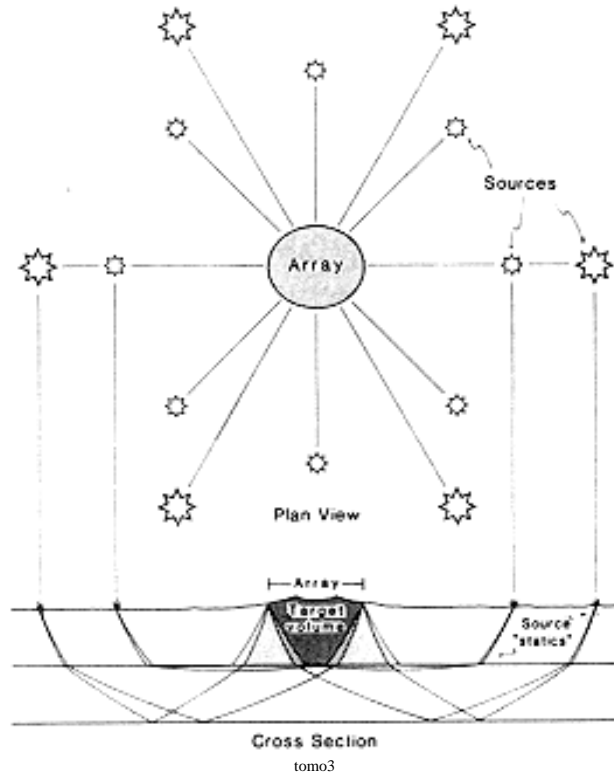
Map view and cross section of NeHT experiment.

Attenuation tomography based on NeHT-principles takes advantage of cancelling effects of the source term and the instrument response (if sensors of the same kind are used) and consider spectral ratios S_{ij}:

$$\ln S_{ij} = \ln(A_{ij}^r A_{ij}^u + B_{ij}^r B_{ij}^u) - \frac{1}{n_i} \sum_{j=1}^{n_i} \ln(A_{ij}^r A_{ij}^u + B_{ij}^r B_{ij}^u)$$

Schematic ray diagram for NeHT-attenuation tomography.

---

[13] Nercessian, A., Hirn, A. & Tarantola, A. 1984. Three-dimensional seismic transmission prospecting of the Mont Dore volcano, France. Geophys.J.R.Astron.Soc., 76, 307-315.

[14] Achauer, U., Evans, J.R. & Stauber, D.A. 1988. High-resolution seismic tomography of compressional wave velocity structure at Newberry Volcano, Oregon Cascade Range. J.Geophys.Res., 93, 135-147.

ATTENUATION TOMOGRAPHY

Seismic attenuation is caused by intrinsic elasticity (small scale dislocations, friction) and scattering (redistribution of seismic energy by reflection, refraction and conversion due to heterogeneities).

type of attenuation	frequency range	wavelength	observed in the
intrinsic inelasticity	low	long	far field
scattering	high	short	near field

The approach is similar those of travel time tomography. In this case, the quality factor 'Q' is introduced:

$$A(f)_i = \exp\left[-f \int_{L_i} \frac{s_j}{Q_j} dl\right]$$

Taking logarithms leads to the same problem as in travel time tomography:

$$-\frac{1}{f} \ln(A(f)_i) = \int_{L_i} \frac{s_j}{Q_j} dl$$

and identical techniques can be used to solve for s_j/Q_j. Thus, knowing the velocity structure $(1/s_j)$, the Q-structure can be determined.

> Attenuation tomography requires a velocity model!

Problems:
1. Amplitude dissipation due to interferences
2. Amplitude decay due to scattering, diffraction and reflection (e.g. on faults)
3. Source spectrum
4. Directivity of source and receiver

Note, hat the intrinsic inelasticity alters the amplitude spectrum by the factor $e^{-\pi f t^*(f)}$ with

$$t^*(f) = \int_L \frac{dl}{v(l)Q(l,f)}$$

Remark: Dispersive effects on the propagation velocity '*v(l)*' along the ray path 'L' are neglected here.

Procedure:

1. Determine the reduction of the amplitude beyond elastic effects. This step might involve assumptions of a source spectrum, scaling laws, etc. Note: negative residuals are indicative for wrong assumptions!
2. Measure the spectral decay of observed body waves relative to the assumed shape.

To estimate stable and absolute attenuation, e.g. core reflections of shear waves (ScS) were used for studies of the Earth's mantle. Reason: ScS-arrivals are a result from similar source radiation angles, hence source effects can mainly be eliminated.

$$F(\omega, \Delta t)S_n(\omega) + N(\omega) = S_{n+1}(\omega)$$

with 'S_n' and 'S_{n+1}' being the spectra of the 'ScS_n' and 'ScS_{n+1}' waves. '$N(\omega)$' is the noise spectrum, and '$F(\omega)$' is the attenuation filter '$exp(-\omega\Delta t/2Q_{ScS})$'. Computing spectral ratios of '$ScS_{n+1}(f)/ScS_n(f)$' eliminates almost the unknown source spectrum.

Another way determining the 't^*'-factor is computing synthetic waveforms and varying 'Q' until the synthetic waveforms match the observed ones. This method requires the knowledge of the instrument response, however.

The example below shows an analysis of 'ScS_n'-reverberations for the determination of the whole-mantle attenuation[15].

Figure (a): Ray paths of multiple 'ScS_n' reverberations

Figure (b): Tangential components of 'ScS_n' phases for the October 24, 1980 earthquake in Mexico

Figure (c): Spectral ratios of successive 'ScS_n' phases, indicating a 'Q_{ScS}' for Mexico of 142.
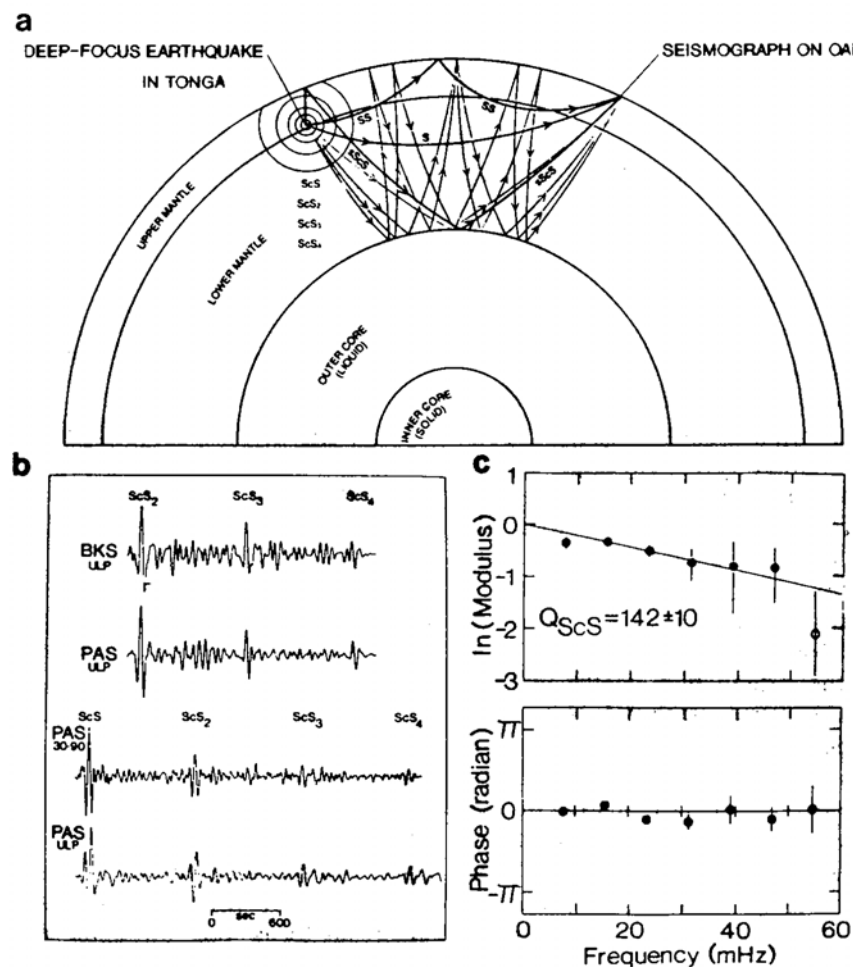
lw0707

---

[15] Lay, T. & Wallace, T.C. 1995. Modern Global Seismology. Academic Press, Inc., page 251.

PROBLEMS IN TOMOGRAPHY

Wavelength and curved ray-paths

The effect of ray-path bending needs to be considered once velocity contrasts exceed 10 - 15 % of the average velocity of the medium - and the size of the disturbance is larger than the seismic wavelength[16].

Wavelength as function of velocity and frequency
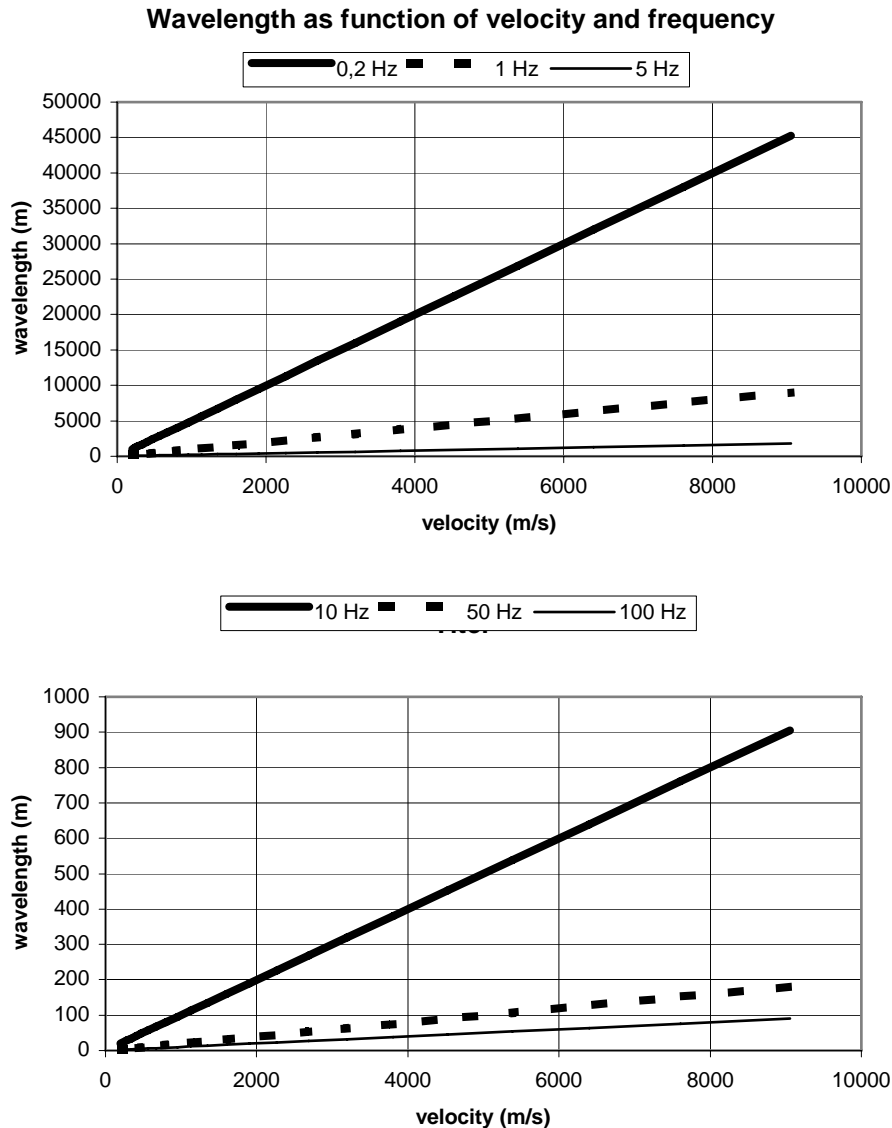
Diffraction and the effect of intrusions

High velocity intrusions appear larger in space, negative velocity anomalies are underestimated, for they are unlikely to manifest themselves in travel time data[17].

Computational limits

The larger number of unknowns, large matrices and the ill-conditioned system poses serious problems, which are consistently reduced by the steady increase of computing power.

---

[16] Kijko, A. 1996, Statistical methods in mining seismology. South African Geophysical Association

[17] Wieland, E. 1987. On the validity of the ray approximation for interpreting delay times. In: Seismic Tomography (Nolet, G., ed.), Reidel, Dordrecht, 85-89.

EARTH STRUCTURE
OVERVIEW
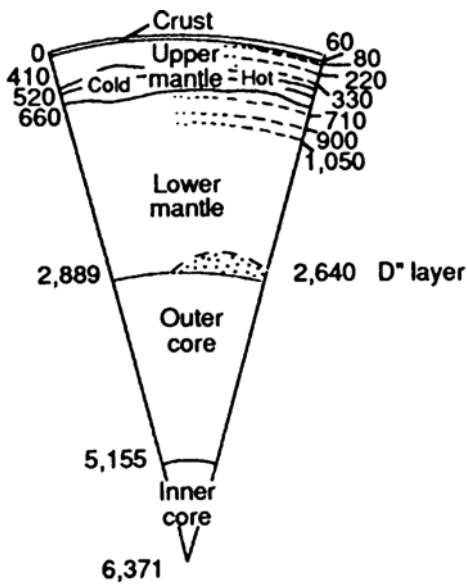
Schematic cross section through the Earth (Nature, Vol.355, pp.768-769)

Region	Level	Depth (km)
-	outer surface	0
A	crust	
-	base of crustal layers, Mohorovicic disc.	33
B	upper mantle	
-		413
C	upper mantle	
-		984
D	lower mantle incl. D'' layer	
-	core-mantle boundary CMB	2898
E	outer core	
-		4982
F	outer core	
-		5121
G	inner core	
-	Earth's centre	6371

Specification of internal shells of the Earth after K.E.Bullen (1942).

lw0120
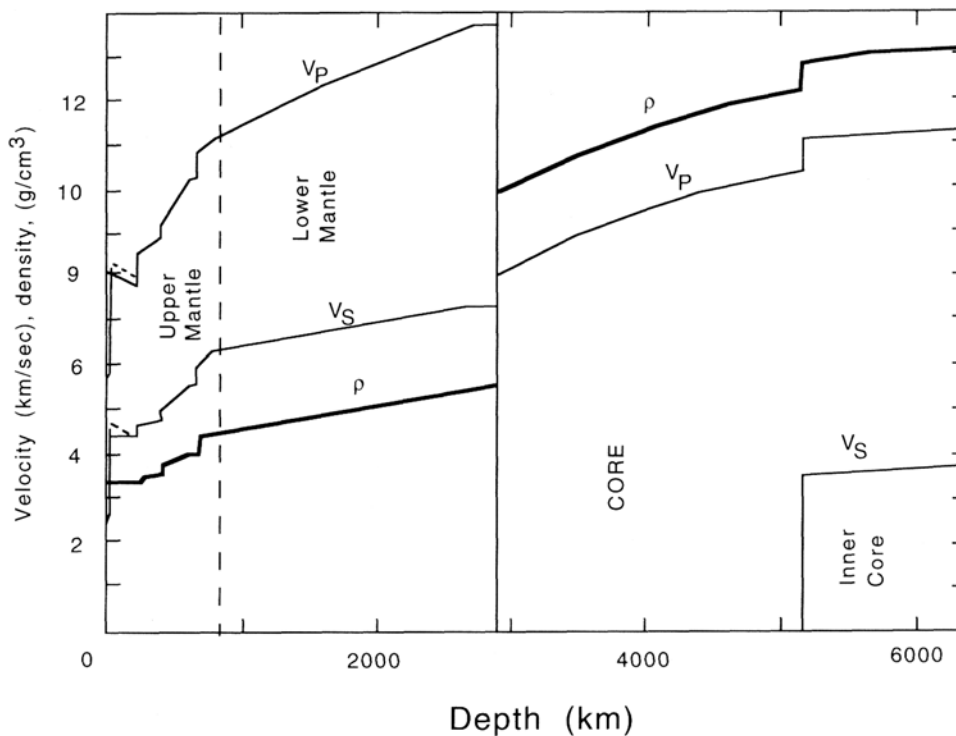
The Preliminary Reference Earth Model (PREM from Dziewonski & Anderson, 1981) shown here is a refined model based on Jeffreys & Bullen (1939)[18].

Note, that terms such as 'lithosphere' and asthenosphere' address dynamic processes rather than seismic velocity properties.

---

[18] see also Bullen, K.E. & Bolt, B.A. 1985. An introduction to the theory of seismology. Cambridge University Press, 4th edition.

CRUST

BASICS

1909	Along with the earthquake in the Kulpa Valley (Croatia) on October 8, 1909, **Mohorovicic** estimated the thickness of the crust to be 54 km. He used P- and S-waves to arrive at this result.
1923	**Conrad** evaluated the Tauern-earthquake (November 28, 1923) and interpreted a 'P*'- wave, which he attributed to be an effect of a transition zone within the crust.
1926	**Jeffreys** studied the Jersey and Hereford earthquake (UK) and introduced the terms 'Pg' and 'Sg' for waves travelling within the 'granitic' crust.
1928	**Stoneley** detected differences between continental and oceanic crust based on the dispersion of Love waves.
1937	**Jeffreys** introduced the terms 'Pg', 'P*', 'Pn' and 'Sg', 'S*', 'Sn'.
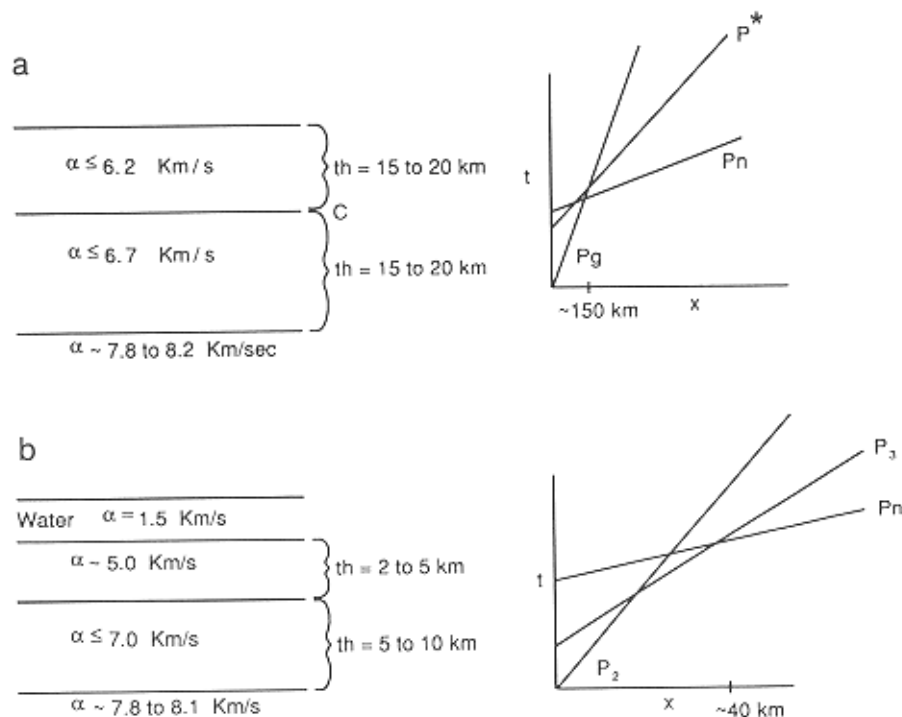
lw0708

Continental versus oceanic crust. Note, 'P$_2$' and 'P$_3$' are the oceanic equivalents of the 'Pg' and 'P*' onsets observed on continental crust[19].

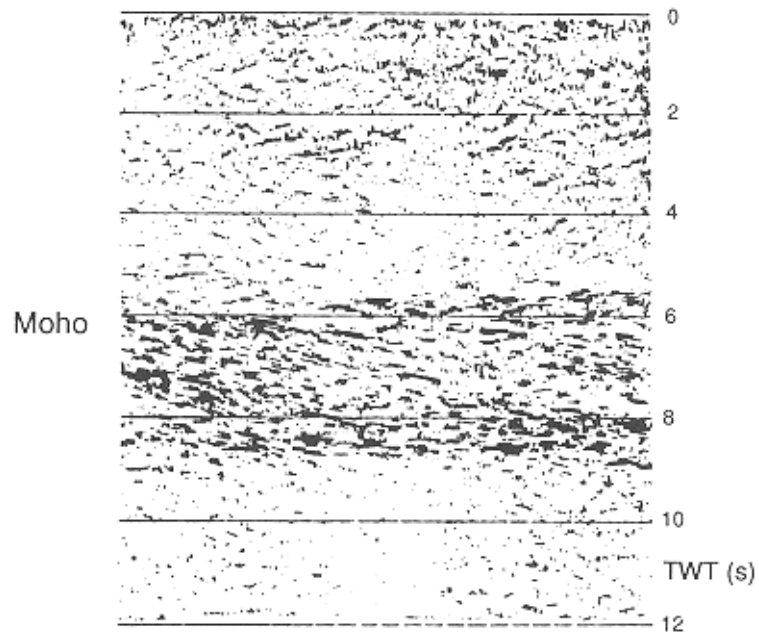[19] Lay, T. & Wallace, T.C. 1995. Modern Global S. Academic Press, Inc.

CRUST

CONTINENTAL CRUST
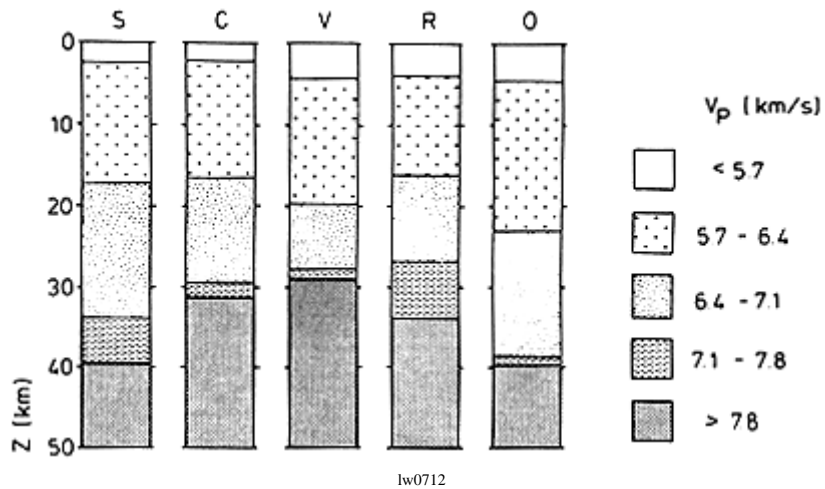
Idealized velocity-depth distributions in various continental crustal provinces. S = shields, C = Caledonian provinces, V = Variscan provinces, R = rifts, O = orogens (from Meissner & Wever, 1989, see Lay & Wallace, 1995)
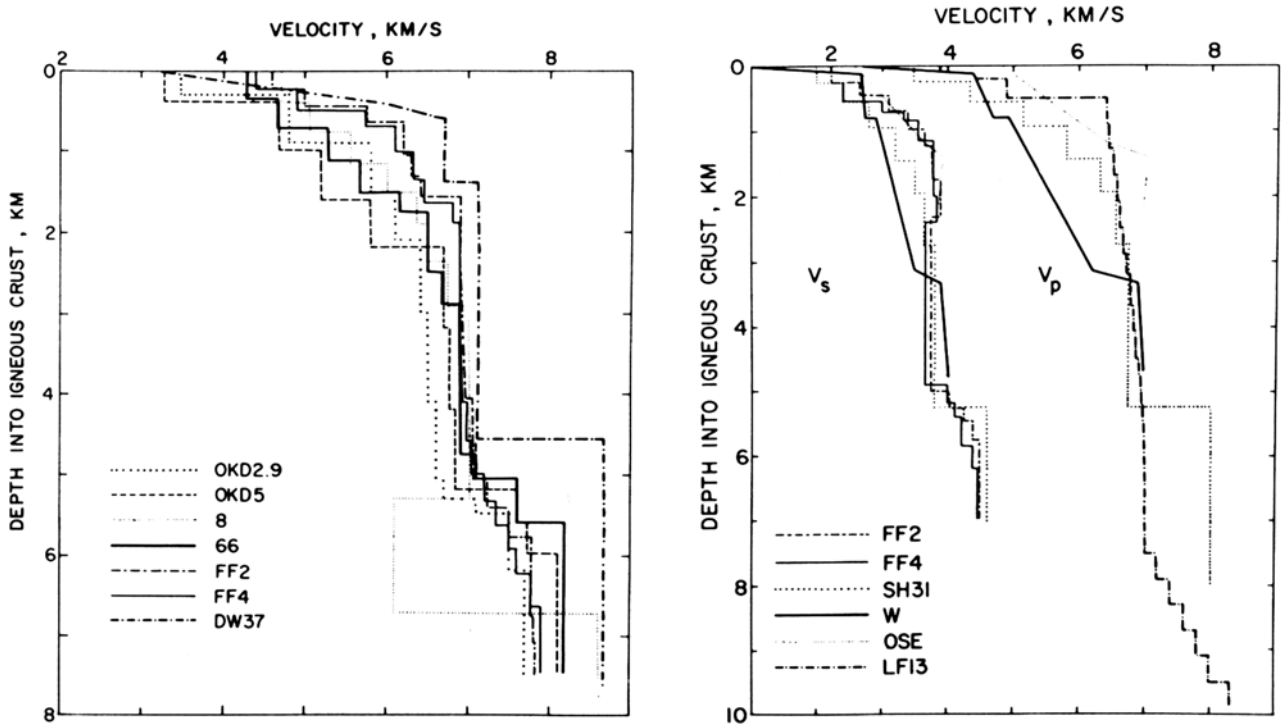

Multiple reflections at two-way travel times (TWT) of 6 - 9 seconds below the Black Forest, Germany, believed to indicate a layered or laminated Moho transition. (from Meissner & Bortfield, 1990, see Lay & Wallace, 1995)

CRUST

OCEANIC CRUST

P-velocity profiles for young oceanic crust (< 20 million years)

P- and S-velocities in older oceanic regimes (> 20 million years)

(in Lay & Wallace, 1995, based on [20])

Note, that the crustal thickness varies less than in continental regions and amounts to 5-7 km in most places.

Exemptions, which account for less than 10% of the oceanic crust are found

1. near fracture zones (thickness ~ 3 km), and
2. beneath oceanic plateaus (thickness up to 30 km)

Although the thickness varies little, 'P_n'-velocities show a dependence on the age of oceanic crust:

1. 7.7 –7.8 km/s near ridges (young material)
2. 8.3 km/s in the oldest Jurassic part of the oceanic crust

Due to the limited thickness of the oceanic crust, relatively high velocity gradients do exist. Cross-over distances between body waves and head waves amount to only 40 km, which is little when compared with the continental crust.

---

[20] Spudich & Orcutt, 1980 in Rev. Geophys. Space Phys., Vol.18, 627-645.

SUBDUCTION ZONES

Subduction zones are mainly found along the **circum-pacific** plate, where also most of the largest earthquakes tend to occur. They are caused by those parts of the <u>oceanic</u> crust which are pushed under adjacent continents. Magnitudes of the largest earthquakes along these subduction slabs appear to correlate with the age of the oceanic crust and its velocity - or convergence rate - according to (Ruff & Kanamori, 1980)

$$M = -0,00889T + 0,134V + 7,96$$

with T = age of plate in millions of years and V = convergence rate in cm/year. Hence, young plates (e.g. 20 million years) with moderate velocities (e.g. 2 cm/year) are capable of generating as large magnitudes as old plates (e.g. 150 million years) with high convergence rates (e.g. 10 cm/year). Subduction zones differ regionally in their down dip extent as well as in the inclination of the subducted slab.
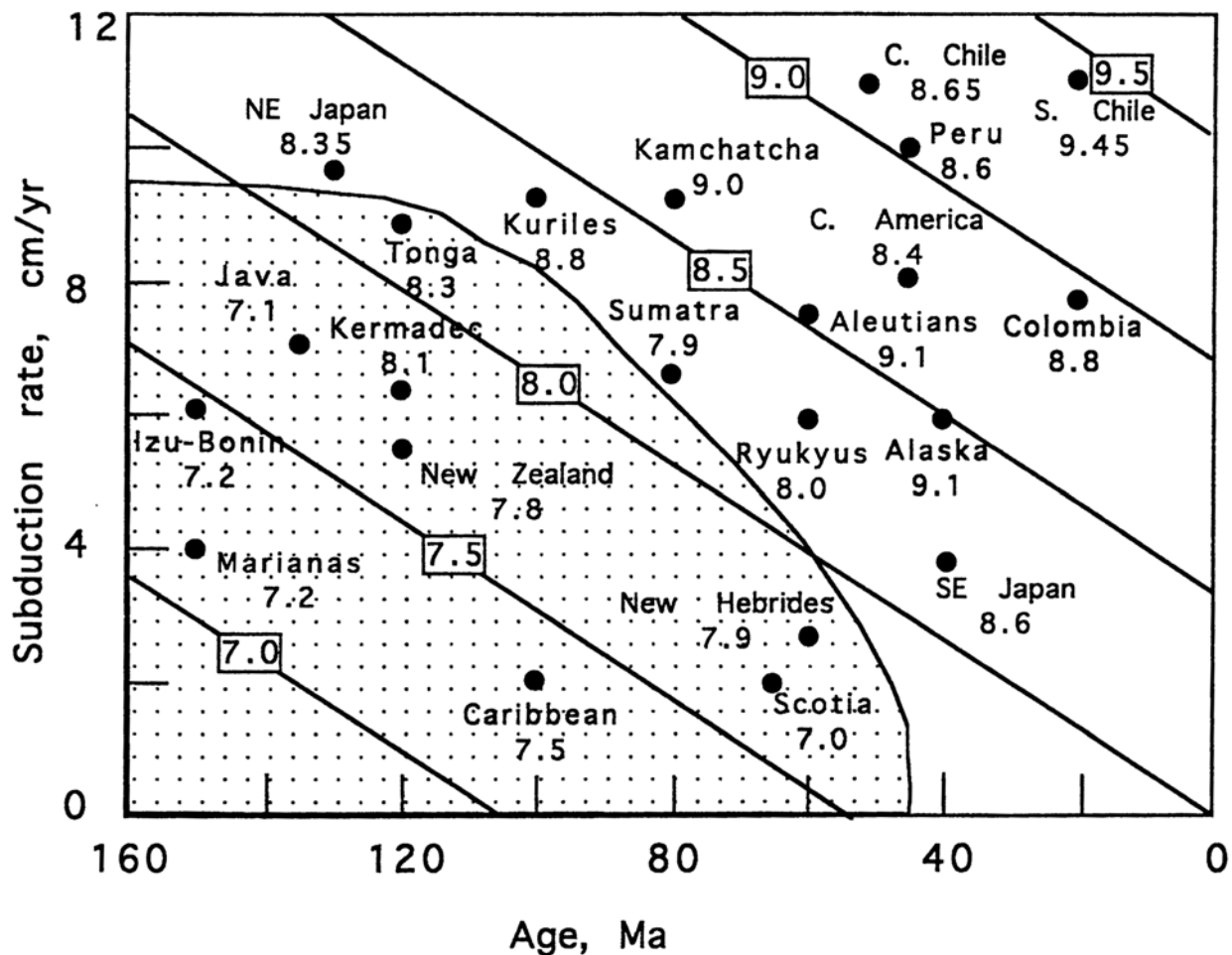
lw1133

Relationship between magnitude of large thrust zones and the age of the subducted lithosphere and the convergence rate. The dashed area delimits the subduction zones which exhibit active back-arc spreading.

Note: The earthquake in 2004 in Sumatra/Indonesia and Tohoku/Japan in 2011 disproved this relation and the conclusions by Ruff & Kanamori (1980)! The issue appears to be much more complicated. This reference is just given because the paper by Ruff & Kanamori (1980) remains frequently quoted.

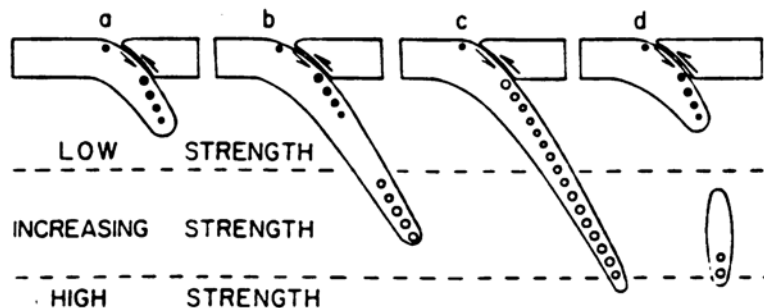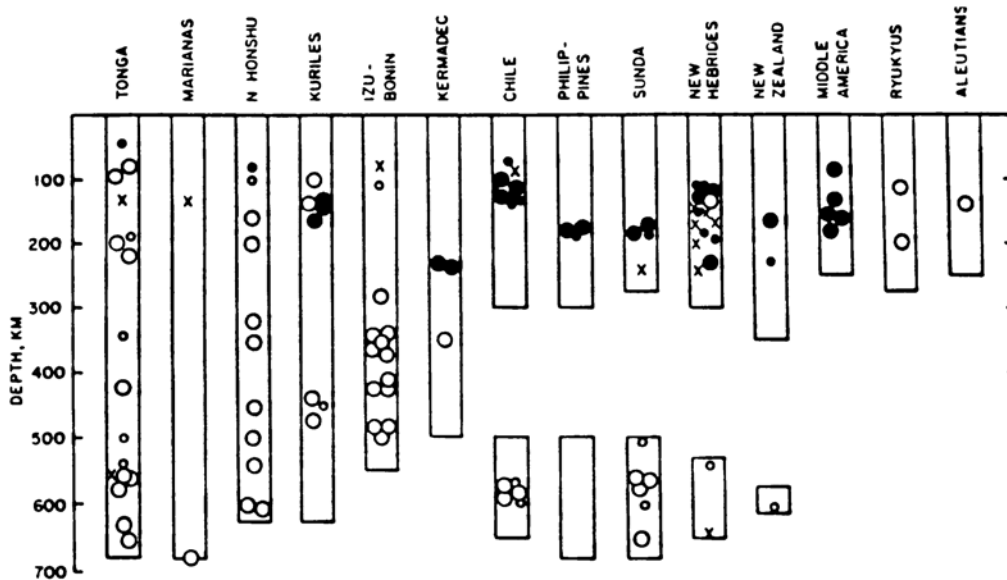Two extreme types of subduction zones may be distinguished:

Chile

Marianas

Asperity model

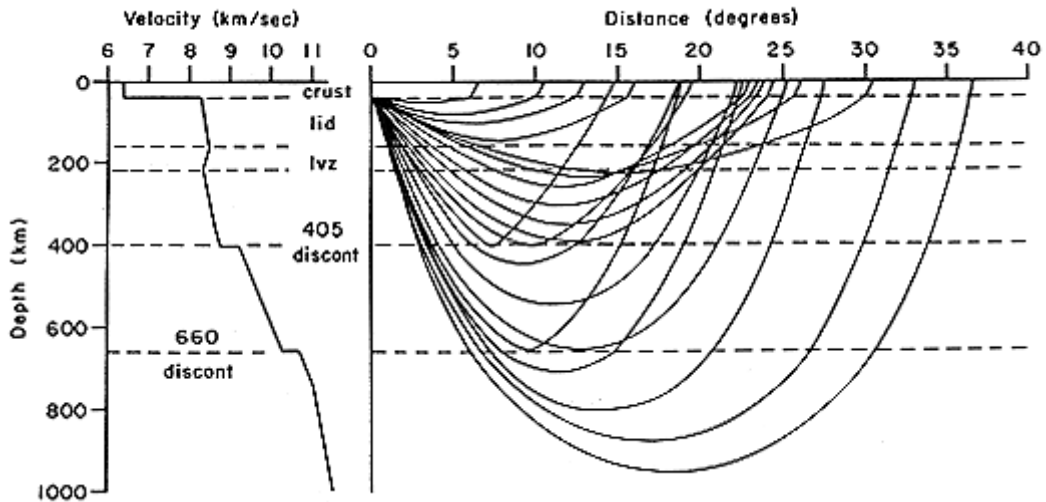|		
Chile		
Aleutians		
Kurile		
Marianas		

⊢⊣ Rupture extent
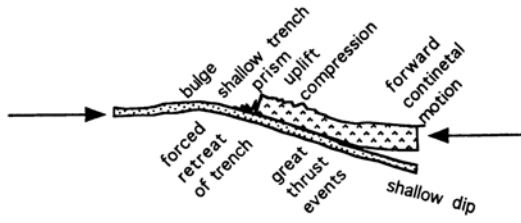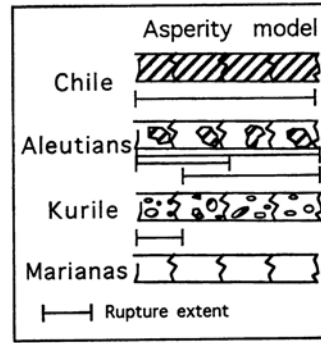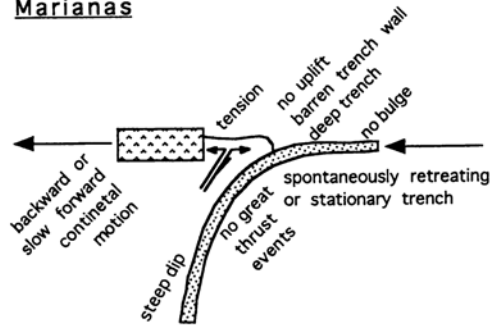
s0611

Down dip extensional (solid) and down dip compressional (open hypocenters) events in various subduction zones (from Isacks & Molnar, 1971 in Lay & Wallace, 1990).

LOW STRENGTH

INCREASING STRENGTH

HIGH STRENGTH

lw1123

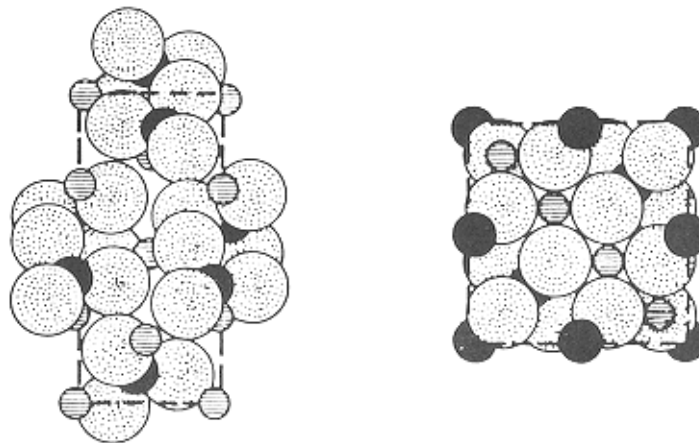These zones of seismicity are also referred to as '**Wadati-Benioff**' zones.

UPPER MANTLE

BASICS

Velocity variations with depth produce complex seismic ray paths. Oceanic and continental structures will have different ray paths. Multiple arrivals between 20° and 25° of distance correspond to triplications due to upper-mantle velocity increases.


One of the major causes of the sudden velocity increase in the upper mantle is phase transformation, in which material collapses to a denser crystal structure. The example above shows a low-pressure olivine crystal (black atoms are magnesium). Its high-pressure version - β-spinel - is shown on the right. The transformation occurs near a depth of approximately 410 km and is understood to be reason for high seismic velocities at that depth.

UPPER MANTLE
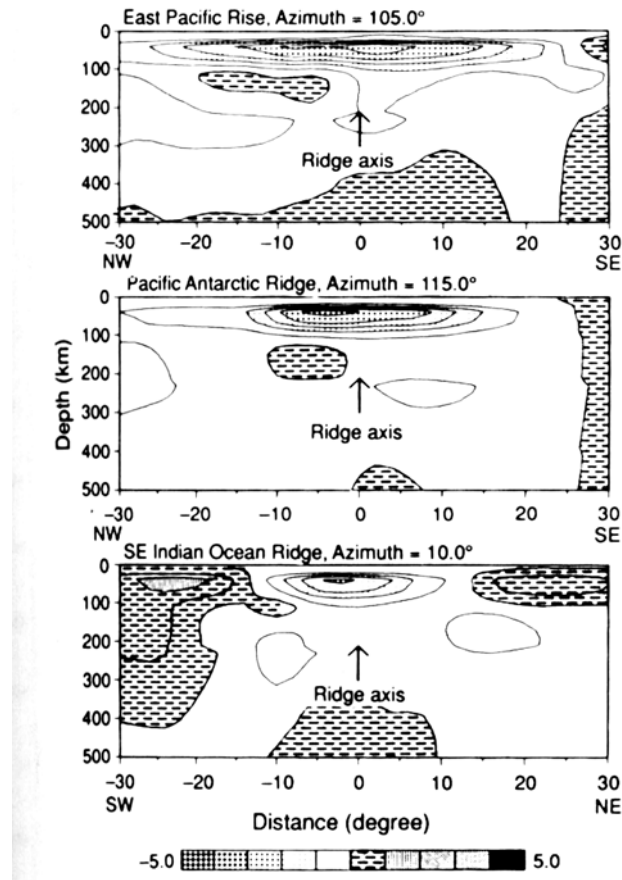
TOMOGRAPHY - THE SAN ANDREAS FAULT
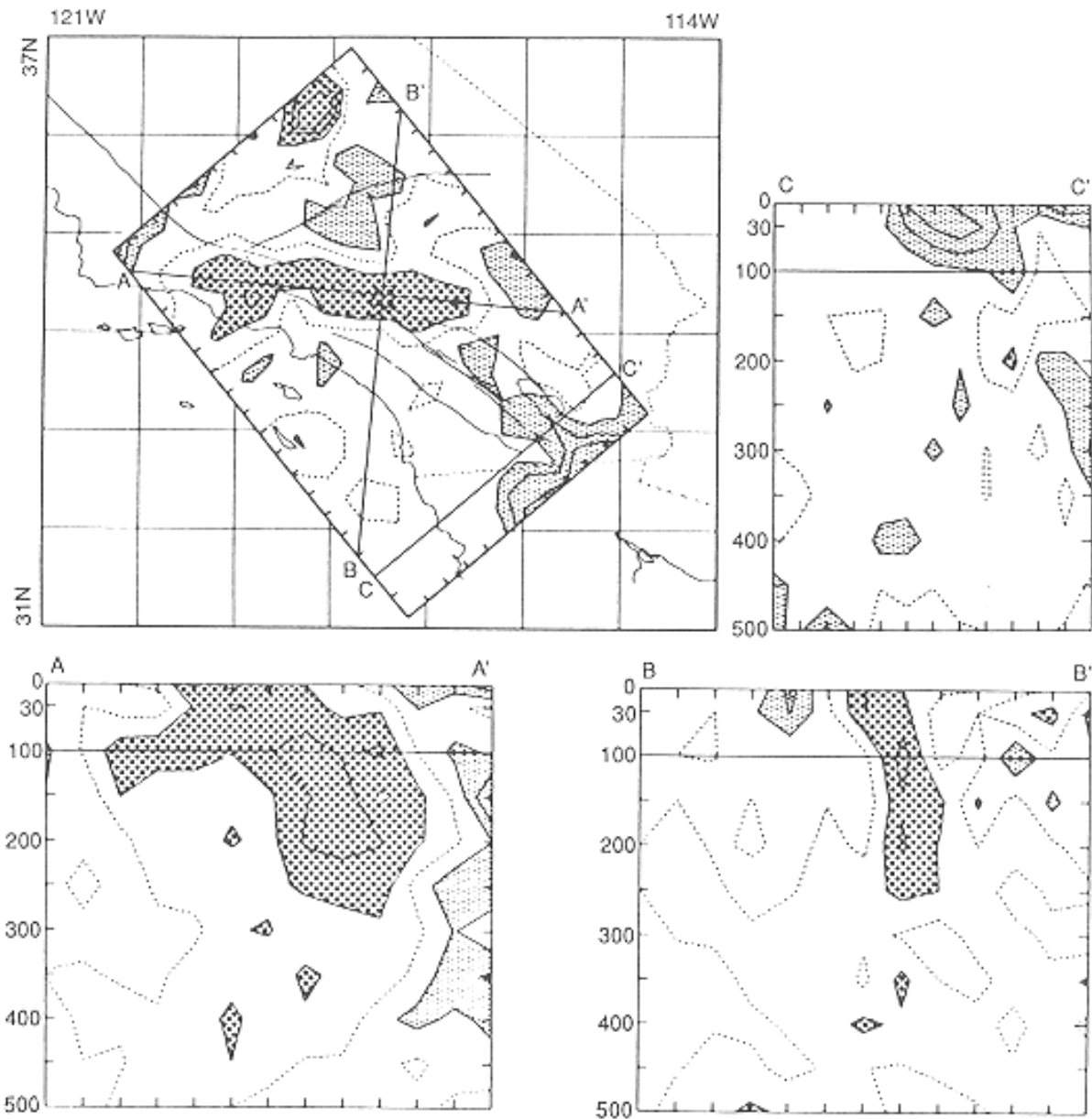
lw0730

Lithosphere heterogeneity under southern California revealed by seismic tomography using P-wave travel times. The dark, stippled region is a fast-velocity body extending almost vertically into the mantle[21].

---

[21] Humphreys et al., 1984, Geophys. Res. Lett., Vol.11, 625-627.
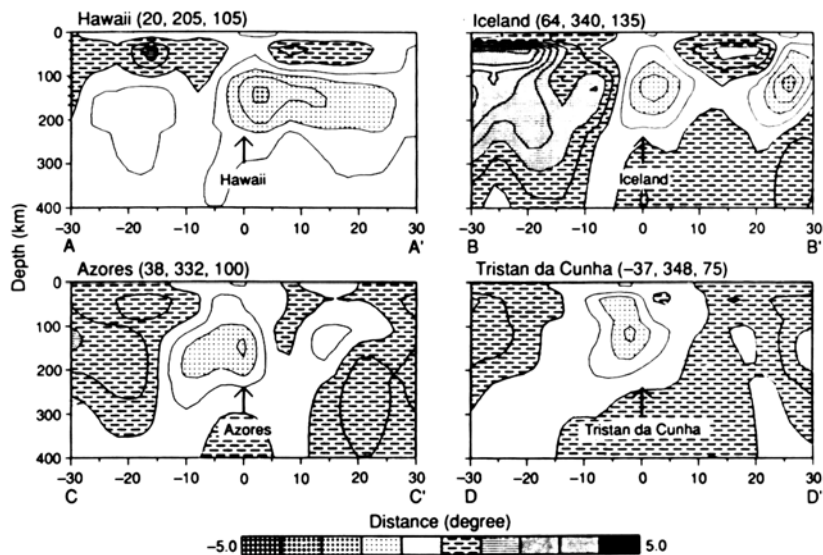
UPPER MANTLE

MID-OCEAN RIDGES

lw0734a

HOT SPOTS

lw0734b

Cross sections of a 3-D shear velocity structure based on Love- and Rayleigh tomography. Dotted regions mark 1% slow shear velocities indicating shallow low-velocity bodies[22].
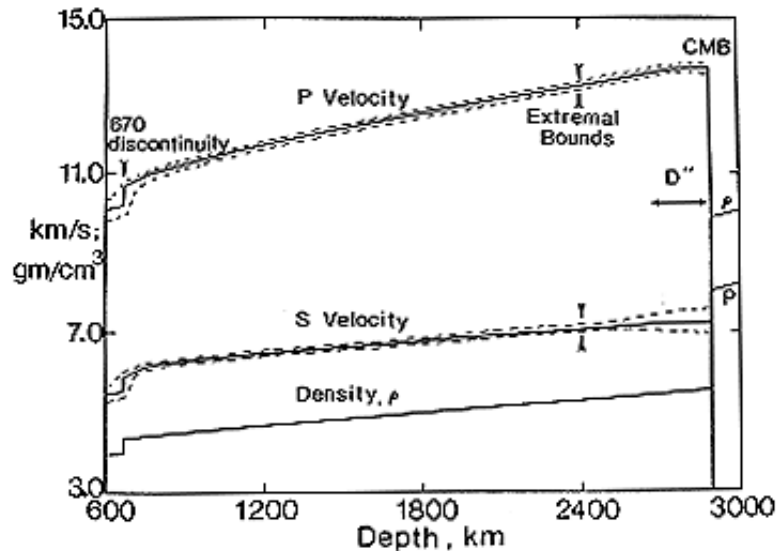
---

[22] from Nature, Vol.355, 45-49, see Lay & Wallace, 1995, page 283.

LOWER MANTLE

BASICS

The lower mantle extends approximately from 600 km to 3000 km below surface. The bottom of the lower mantle is called the core-mantle boundary (CMB).

lw0742

Average lower-mantle seismic velocities and densities. No radial structures are apparent between a depth of 1000 to 2600 km. Then, a 200-300 km thick D'' layer at the base of the mantle shows strong lateral and radial heterogeneity[23].

Hence, the lower mantle (710 to 2600 km depth) may be considered as a layer with consistent velocity gradient and no dominating radial structures or layers. This fact can be ascertained by travel time observations.

Some observations indicate a possible impedance boundary between 900 and 1050 km of depth, however.

---

[23] from Lay, 1989 in Lay & Wallace, 1995, page 292.

LOWER MANTLE

DIFFRACTED WAVES
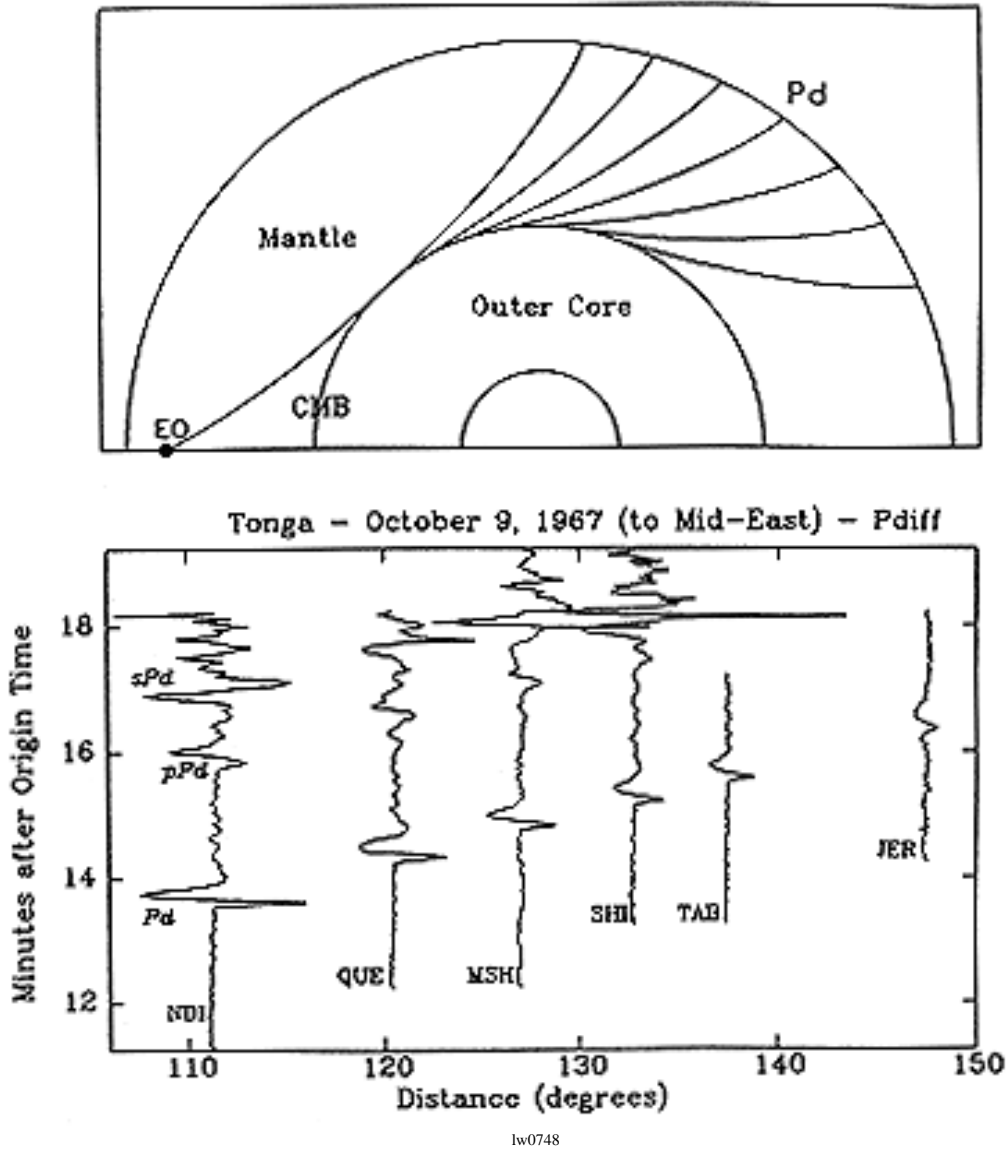
P-waves, diffracted by the outer core, are sampling the lower mantle. Those waves arrive in the so-called 'shadow zone'. Timing and waveforms are subjected to the conditions at the base of the mantle (see also D''-layer)[24].

---

[24] Wysession et al., 1992 in J. Geophys. Res., Vol. 97, 8749-8764.

THE CORE

1906	**Oldham** discovers the core
1912	**Gutenberg** determines depth at 2900 km
1926	**Jeffreys** shows absence of S-waves
1936	**Lehmann** postulates an inner- and an outer core
1938	**Gutenberg & Richter** support Lehmann's hypothesis
1970	Solidicity of inner core accepted
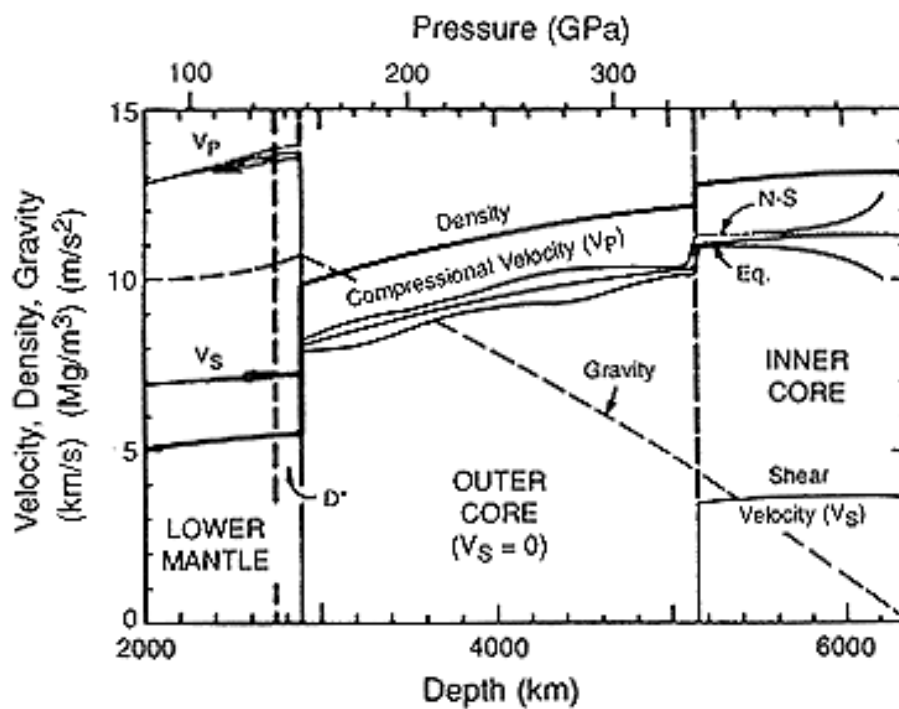
lw0751

Seismological determined densities (10^3 kg/m³ - bold solid curve), P- and S-wave velocities (km/s - thin solid lines) and gravitational acceleration (m/s² - thin dashed curve) as function of depth (bottom scale) and pressure (top scale). 'N-S' and 'Eq.' denote polar and equatorial compressional velocities, respectively. Note, D''-layer at the core-mantle boundary (CMB)[25].

---

[25] Jeanloz, 1990, in Annual Rev. of Earth and Planet. Sciences, Vol.18, 357 - 386.